THE JOURNAL OF PHYSICAL CHEMISTRY B

pubs.acs.org/JPCB Article

Examining Tail and Headgroup Effects on Binary and Ternary Gel-Phase Lipid Bilayer Structure

Alexander Yang, Timothy C. Moore, Christopher R. Iacovella, Michael Thompson, David J. Moore, and Clare McCabe*

Cite This: J. Phys. Chem. B 2020, 124, 3043−3053 Read Online

ACCESS | Metrics & More | Article Recommendations | Supporting Information

ABSTRACT: The structural properties of two- and three-component gel-phase bilayers were studied using molecular dynamics simulations. The bilayers contain distearoylphosphatidylcholine (DSPC) phospholipids mixed with alcohols and/or fatty acids of varying tail lengths, with carbon chain lengths of 12, 16, and 24 studied. Changes in both headgroup chemistry and tail length are found to affect the balance between steric repulsion and van der Waals attraction within the bilayers, manifesting in different bilayer structural properties. Lipid components are found to be located at different depths within the bilayer depending on both chain length and headgroup chemistry. The highest bilayer ordering and lowest area per tail are found in systems with medium-length tails. While longer tails can enhance van der Waals attractions, the increased tail-length asymmetry is found to induce disorder and reduce tail packing. Bulkier headgroups further increase steric repulsion, as reflected in increased component offsets and reduced tail packing. These findings help explain how bilayer composition affects the structure of gel-phase bilayers.

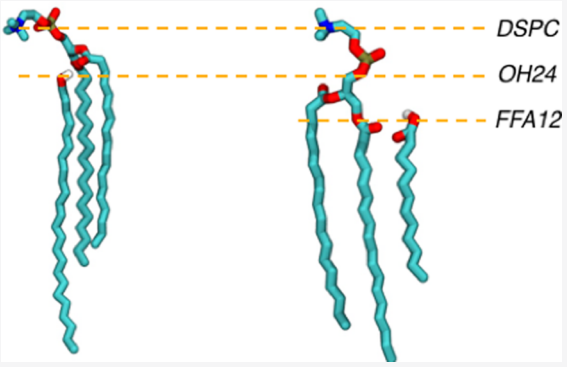

INTRODUCTION

Phospholipids are often a key component in cosmetic and pharmaceutical formulations used as topical treatments designed to retain moisture by mimicking the barrier function of healthy skin. The excellent barrier properties of healthy skin[1−4] have been attributed to the dense, gel-phase ordering exhibited by the lipids found in the outermost layer (i.e., the stratum corneum). While phospholipids with unsaturated tails typically form bilayers in the liquid-crystalline phase, those with fully saturated tails, as often found in topical treatments, have been observed to occupy a gel phase in which the lipids are highly ordered and fairly immobile.[5] While the stratum corneum is largely composed of ceramide compounds, various synthetic formulations that include phospholipids have been shown to contribute to the gel-phase behavior of the stratum corneum and improve barrier function as both a component that incorporates into the stratum corneum and a component that forms an external gel-phase layer; this work focuses on the latter.[3,6−11] Designing such formulations is a nontrivial task, as it requires an understanding of how the individual lipids in the formulation—and their relative composition and tail lengths—influence the structure and properties of the bilayer.

To date, several experimental methods have been utilized to study the structure and properties of gel-phase lipid bilayers. Early observations of various bilayer phases were reported by Tardieu et al., who characterized lattice parameters and tilt angles in gel and tilted-gel phases.[5] Work by Lis et al. characterized the force between different gel-phase bilayers as a function of separation distance, identifying an exponentially decaying "hydration repulsion", which was found to depend on phospholipid polar groups and packing of the hydrocarbon acyl chains.[12] Later, Rand and Parsegian explored water uptake and bilayer properties versus relative humidity, rationalizing the behavior via hydration, electrostatic, undulation, steric, and van der Waals forces and noting that hydration forces help drive phase transition behavior and bilayer order.[13] The hydration force was used by Smith et al. to explain changes to bilayer thickness, hydrocarbon tilt, and surface area per headgroup.[14] Sun et al. utilized low-angle and wide-angle X-ray scattering experiments to study gel-phase, saturated lipids, observing increases in area per chain, tilt angle, and bilayer thickness as lipid chain length increases.[15−17] Using electron density studies, Wiener et al. were able to determine methylene and headgroup volumes, bilayer thicknesses, and hydration within

Received: January 17, 2020
Revised: March 20, 2020
Published: March 20, 2020

gel-phase phospholipid bilayers, demonstrating the utility of electron density modeling to examine gel-phase bilayers.[18]

Experimental lipid bilayer studies have also considered mixed lipid systems. For example, Hishida et al. in numerous studies observed that the addition of *n*-alkanes can rigidify bilayers, alter bilayer transition temperatures, and also influence phase separation.[20−22] Aagaard et al. observed the ability of alkanes and alcohols to affect fluid-phase bilayer packing properties and volume in different ways depending on chain length relative to the bilayer-forming lipid (14 carbons).[23] Ingolfsson and Andersen further explored this property with longer bilayer-forming lipids (22 carbons) and a greater variety of alcohol chain lengths, identifying the different behaviors between short- and long-chain alcohols when looking at how alcohols stabilize membrane−protein interactions.[24] Additional experiments have demonstrated the ability of short-chain alcohols to disorder and disrupt the structural and mechanical properties of fluid-phase lipid membranes.[25,26] In fluid-phase systems, cholesterol is known to increase orientational order in phospholipid tails, reduce lipid lateral diffusion, improve packing, and thus influence solute permeability,[27] although the opposite is observed in gel-phase systems.[28] Other experimental evidence suggests that the addition of fatty acid components can alter the morphology of pure gel-phase phospholipid systems from tilted and rippled phases into untilted, gel phases.[29] Thus, there is evidence that mixed, gel-phase bilayers can demonstrate properties different from their pure, gel-phase counterpart; furthermore, the mixture behavior can be different in gel-phase systems compared to fluid-phase systems.

While it is clear a relationship exists between composition, structure, and function in pure and mixed gel-phase phospholipid-based bilayer systems, there is a lack of molecular understanding with respect to how different components affect bilayer structure. In this regard, molecular simulation can be a powerful tool, providing direct access to atomic spatial coordinates and interactions over time as well as serving as an effective platform for a systematic comparison of similar systems with slightly different compositions. While there is extensive simulation literature for fluid-phase lipid bilayers, we restrict our focus to simulations of gel-phase lipid bilayers. Early simulations of gel-phase phospholipid (dipalmitoylphosphatidylcholine, DPPC) bilayers were conducted by Tu et al.[30] and Essman et al.,[31] who examined areas per lipid, density profiles, and chain configurations for simulations up to 1 ns, which as noted by the authors was too short to demonstrate convergence.[30] Poger et al. later introduced the GROMOS53A6 parameter set and examined the structural properties of gel-like DPPC bilayers.[32] Hartkamp et al. used this force field to report a range of gel-phase bilayer properties for 1,2-distearoyl-*sn*-glycero-3-phosphocholine (DSPC) and mixed DSPC−alcohol systems, noting that the larger DSPC headgroups introduced greater steric repulsions and increased bilayer area per lipid, while longer alcohol tails resulted in greater van der Waals attractions, increased tilt angle, and improved lipid tail packing.[33−35] While the GROMOS force field was shown to describe gel phase lipids well, issues were reported with the CHARMM lipid force field that were addressed in numerous force field updates.[36−42] Most recently, Klauda et al. introduced CHARMM36 to better parametrize lipids and reproduce gel-phase properties, including area per lipid, tail order parameters, and accuracy in tensionless ensembles.[41,43] The CHARMM36 force field has been applied to study a variety of phospholipid-based bilayers and examine, for example, the influence of cholesterol on bilayer properties[44] and phase transition temperatures of saturated phospholipid bilayers.[45] While force fields have been improved and computational resources expanded, allowing for longer simulation times to be studied which is important in gel-phase systems, to the authors' knowledge there have been few simulation studies to date[33−35,46] that examine the influence of composition on the structure of gel-phase phospholipid bilayers as reported herein.

Here, we perform molecular dynamics (MD) simulations to examine the structural behavior of multicomponent gel-phase bilayers of DSPC with various amounts of free fatty acid (FFA) and long-chain alcohol (OH) molecules. Two- and three-component mixtures of DSPC, OH, and FFA were examined. The two-component mixtures consisted of either 33 or 50 mol % DSPC, with the remainder either OH or FFA. The three-component mixtures consisted of either 33% or 50% DSPC, with the remainder equimolar OH and FFA. In all mixtures, OH and FFA tail lengths were either 12, 16, or 24 carbons, abbreviated as OH12, FFA12, OH16, etc.

METHODS

All of the bilayer systems studied were initialized by using the open-source mBuild software package.[47] Each bilayer was constructed using two leaflets consisting of molecules arranged in an 8 × 8 square lattice. Lattice spacing was chosen to be ∼20% larger than the final area per lipid based on earlier work.[33,34] To assess finite system size effects, larger simulations using 10 × 10 leaflets for select compositions were also performed, and good agreement with the 8 × 8 leaflets was obtained, suggesting that the smaller, more computationally efficient systems can be reliably used. Lipids were initially tilted randomly between 5° and 25° with respect to the bilayer normal and randomly placed at lattice sites. Lipids were also randomly spun around their tail vectors to avoid artificial alignment, as found in other work.[48] Bilayers were solvated with 20 water molecules per lipid for a total of 2560 water molecules for 8 × 8 leaflet systems. Energy minimization was performed using steepest descent to remove any unfavorable overlaps between molecules in the initial configuration followed by 100 ps of NVT equilibration and 500 ps of NPT equilibration. Random walk MD (RWMD)[49] was then performed for a total of 190 ns to relax the bilayer configurations away from any initial configuration bias. Briefly, RWMD involves a random walk through a predefined temperature space over the course of a MD simulation by randomly swapping simulation temperatures with adjacent temperatures.[49] For the first 30 ns, temperature windows were spaced 10 K between 305 and 455 K. For the remainder of the RWMD, the temperature ceiling (initially 455 K) was reduced by 10 K every 10 ns to allow the system to gradually settle into a stable, gel-phase configuration at 305K. 100 ns of NPT sampling was then performed at 305 K and 1 bar, with the last 20 ns used for analysis. Over the 100 ns of NPT sampling, systems were determined to be well-equilibrated based on agreement between leaflet angle distributions, convergence of measured values over time, and agreement of measured values across simulations of the same composition from three initial configurations with randomized in-plane organization, tilt angle, rotation about the tail axis,[48] and area per lipid.

All simulations were performed using the GROMACS 2018 MD simulation engine.[50−56] DSPC, alcohol (OH), and free

https://dx.doi.org/10.1021/acs.jpcb.0c00490
J. Phys. Chem. B 2020, 124, 3043−3053

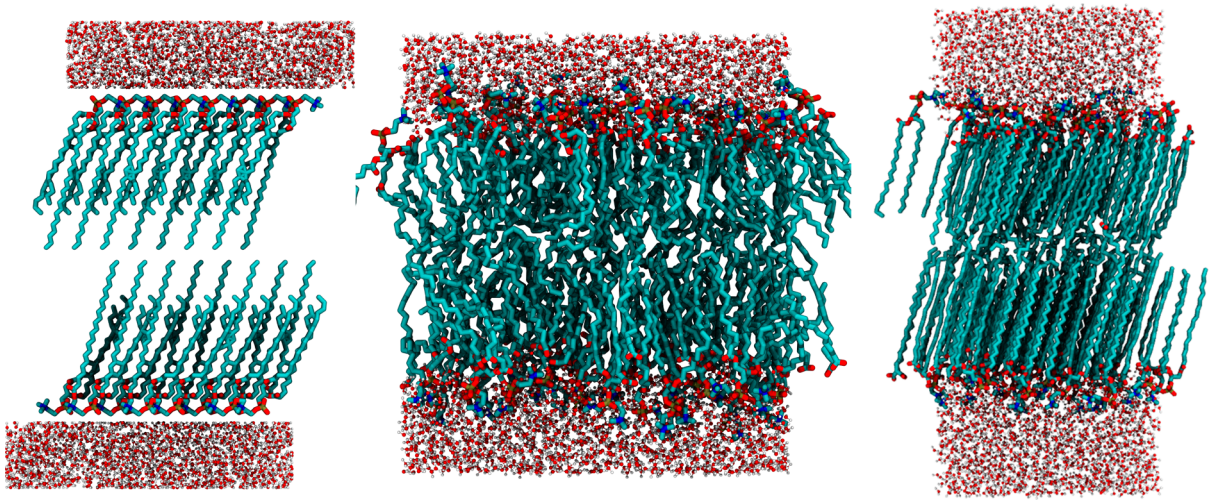

Figure 1. 1:1 DSPC-FFA24 configurations during the equilibration protocol: mBuild-generated structure (left), sample configuration from RWMD (middle), and relaxed, gel-phase structure (right).

fatty acid (FFA) molecules were parametrized according to CHARMM-GUI in accordance with the CHARMM36 all-atom force field.[57,58] Water was modeled using the TIP3P force field and constrained with the SETTLE algorithm.[59−61] All other bonds containing hydrogen were constrained by using the LINCS algorithm.[62] Electrostatics were computed by using the particle mesh Ewald (PME) method with a real-space cutoff of 1.2 nm and a Fourier spacing of 0.16 nm.[63] Force-switching functions were used for van der Waals interactions between 10 and 12 Å.[57] The temperature was held at 305 K by using a Nosé−Hoover thermostat with a 1.0 ps time constant.[57,64,65] Pressure was held semi-isotropically at 1 bar (*XY* and *Z* directions coupled separately) by using a Parrinello−Rahman barostat with a 2.0 ps time constant.[66] Compressibility was held at 4.5×10^{-5} bar^{-1}. A 2 fs time step was used. Snapshots throughout the equilibration process are shown in Figure 1.

■ ANALYSIS

Atomic positions and simulation box dimensions were used to compute the area per lipid (APL), area per tail (APT), average tilt angle, component offset distances, bilayer height, and interdigitation. The APL was computed by dividing the cross-sectional area of the simulation box by the number of lipids in the leaflet. The tilt angle was taken as the angle between the long axis of a molecule's tail and the bilayer normal, with the long axis defined as the eigenvector corresponding to the minimum eigenvalue of the inertia tensor, averaged over all tails.[67] The APT was computed by dividing the APL by the average number of tails per lipid and multiplying by the cosine of the average tilt angle of the entire system, yielding one APT value for the entire bilayer. Component offset distances were determined by comparing the average depth (*z*-coordinate) of the DSPC phosphate group's center of mass and the component's headgroup center of mass. For alcohol (OH) groups, the headgroup was taken as the hydroxyl group. For fatty acids, the headgroup was taken as the carboxylic acid group. For convention, a component with a larger offset is buried deeper into the bilayer. The bilayer height was computed as the average offset distance of DSPC phosphate groups between leaflets. Interdigitation (I_{dig}) was calculated by using the overlap between leaflet density profiles via eq 1,[68]

$$I_{dig} = \int_{-\infty}^{\infty} \frac{4\rho_T(z)\rho_B(z)}{(\rho_T(z) + \rho_B(z))^2}\, dz \quad (1)$$

where the subscripts "T" and "B" indicate the top and bottom leaflets, respectively. The *S*2 order parameter was computed as the largest eigenvalue of the nematic tensor, derived from the lipid tails in each leaflet.[49,69] Block averaging was performed with block sizes of 5 ns. Error bars are reported as 1 standard error from the block-averaging procedure. Simulation analyses were conducted using the MDTraj and MDAnalysis Python libraries.[70−72] Analysis was aided by software packages within the scientific Python ecosystem: SciPy,[73] NumPy,[74] Pandas,[75] and Matplotlib.[76]

■ RESULTS AND DISCUSSION

To validate the simulation methodologies used, a single-component DSPC bilayer was first studied. Results for the pure DSPC system are presented in Table 1 and are found to be consistent with both experiment (Sun et al.)[16] and simulation (Hartkamp et al.[34] and Khakbaz et al.[45]). We note that the simulations of Hartkamp et al. for DSPC used a similar simulation protocol (specifically RWMD) but the GROMOS53A6 force field. Khakbaz et al. used the same force field as in this work (i.e., CHARMM36); however, they studied dipalmitoylphosphatidylcholine (DPPC). DPPC has the same headgroup as DSPC but two fewer carbons in each tail; thus, we expect DSPC and DPPC to have similar APL and tilt values

Table 1. Structural Data for a Pure DSPC Bilayer

source	APL (Å^2)	tilt (deg)	APT (Å^2)	height (Å)
this work, DSPC	50.4 (0.1)	35.9 (0.2)	20.3 (0.03)	46.6 (0.1)
Sun et al.,[16] DSPC	47.3 (5)	32.5 (4)	19.8 (1)	47.0 (4)
Sun et al.,[16] DPPC	47.3 (3)	31.6 (4)	20.2 (2)	42.8 (2)
Nagle et al.,[15] DPPC	47.3	32.0	20.1	45.2
Hartkamp et al.,[34] DSPC	49.7 (0.2)	36.3 (0.4)	20.0 (0.1)	48.4 (1.6)
Khakbaz et al.,[45] DPPC	49.6 (0.5)	36.1 (0.6)		44.7 (0.4)

https://dx.doi.org/10.1021/acs.jpcb.0c00490
J. Phys. Chem. B 2020, 124, 3043−3053

and for DPPC to exhibit a smaller bilayer height, which the results support. The agreement obtained also validates the specific simulation protocol used in this work (i.e., RWMD) for the simulation of the gel-phase DSPC systems.[16,34,45]

The results from simulations of two-component mixtures are presented below for each of the key analysis metrics examined. In general, we find that the bilayer properties are largely determined by the fraction of DSPC in the system and the tail lengths of the FFA and/or OH molecules, with headgroup differences between FFA and OH causing modest differences in structure.

Component Offset Distances. Because of the large steric repulsions from DSPC headgroups, in mixed lipid systems secondary components are pushed deeper into the center of the bilayer resulting in component offset distances; a schematic illustrating the offset between DSPC and a secondary component (i.e., FFA or OH) is shown in Figure 2. Longer

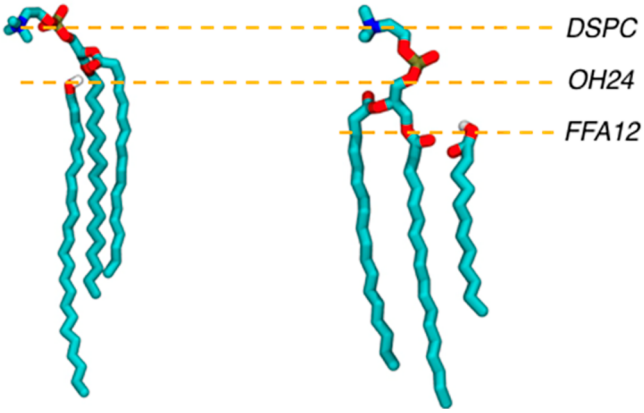

Figure 2. Visualization of component offsets from simulations of (1:2) DSPC-OH24 and (1:2) DSPC-FFA12. The longer lignoceryl (OH24, left) alcohol component lies closer to the DSPC headgroups compared to the shorter dodecanoic acid (FFA12, right) component.

components demonstrate lower offsets, in which the headgroups of longer components reside nearer to the bilayer–water interface. Shorter components, on the other hand, demonstrate greater offsets, in which headgroups are found deeper within the bilayer. Plots of the offsets observed in binary mixtures between DSPC and a secondary component are presented in Figure 3. The component offset is observed to be most strongly dictated by the DSPC fraction and the tail length and, to a lesser degree, the identity of the second component. To maintain tail overlap, longer chains are found

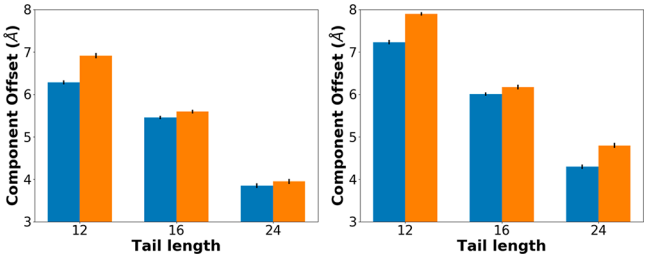

Figure 3. Secondary component offset comparisons for two-component mixtures containing 33% DSPC (left) or 50% DSPC (right). Alcohol systems are shown by blue bars and fatty acid systems in orange.

closer to the bilayer–water interface, whereas shorter chains are found deeper within the bilayer. For example, for DSPC-FFA12 and DSPC-FFA24, offsets are 6.91 and 3.95 Å, respectively, in a 33% DSPC mixture. Generally, the offset for a FFA tends to be slightly larger than that of an OH, presumably due to the FFA components exhibiting slightly more steric repulsion than OH components due to their larger headgroup. Tabulated values for the offsets obtained are reported in Table S1 of the Supporting Information.

Similar to two-component systems, the three-component systems studied exhibited greater offset with larger DSPC fractions, as these provide greater steric repulsion (Figure 4).

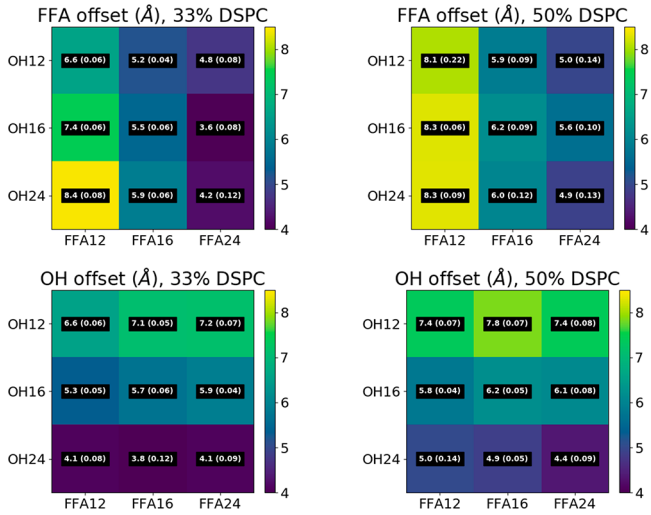

Figure 4. Offset comparisons for three-component mixtures containing 33% DSPC (left) or 50% DSPC (right). Fatty acid component offsets (top) and alcohol component offsets (bottom).

Additionally, shorter-tailed components were again found to have larger offsets, sitting deeper in the bilayer, than longer-tailed components. Comparing corresponding two- and three-component systems with symmetric short tails, i.e., DSPC-OH12, DSPC-FFA12, and DSPC-OH12-FFA12, the component offsets were found to be approximately the same, specifically, 6.29, 6.91, and [6.56, 6.59] Å, respectively, for 33% DSPC and 7.23, 7.90, and [7.37, 8.05] Å, respectively, for 50% DSPC. Similar behavior is seen when considering long-chain symmetric systems, for example, for DSPC-OH24, DSPC-FFA24, and DSPC-OH24-FFA24, where offsets are 3.85, 3.95, and [4.09, 4.24] Å, respectively, for 33% DSPC and 4.29, 4.80, [4.35, 4.90] Å, respectively, for 50% DSPC. Overall, for symmetric cases, relatively small differences in component offsets between binary and ternary mixtures are observed, suggesting that binary mixtures can be predictive of this packing motif.

When considering three-component systems with asymmetric tail lengths, component offsets are found to be slightly larger than the respective binary systems. For example, the offsets obtained for components in the DSPC-OH12-FFA24 system (i.e., [7.15, 4.75] Å for OH and FFA, respectively, for 33% DSPC) are slightly larger as compared to the corresponding binary DSPC-OH12 and DSPC-FFA24 systems (6.29 and 3.85 Å, respectively, for 33% DSPC). Swapping the length of the components shows similar behavior; i.e., DSPC-OH24-FFA12 has offsets [5.03, 8.31] Å for OH and FFA, respectively, as compared to 4.29 and 7.90 Å for DSPC-OH24

https://dx.doi.org/10.1021/acs.jpcb.0c00490
J. Phys. Chem. B 2020, 124, 3043–3053

and DSPC-FFA12, respectively, for 33% DSPC. By increasing the variety of tail lengths present in the three-component bilayers, the lipids can offset slightly differently to maximize tail overlap as compared to the two-component case. Overall, it appears that by lengthening the chain length of one component, the other component can descend deeper into the bilayer. However, we note that 24-carbon tails do not create the same space for molecules to descend due to the loss of nematic order toward the middle, interdigitated region of the bilayer (see Figure 5). The loss in nematic order can be

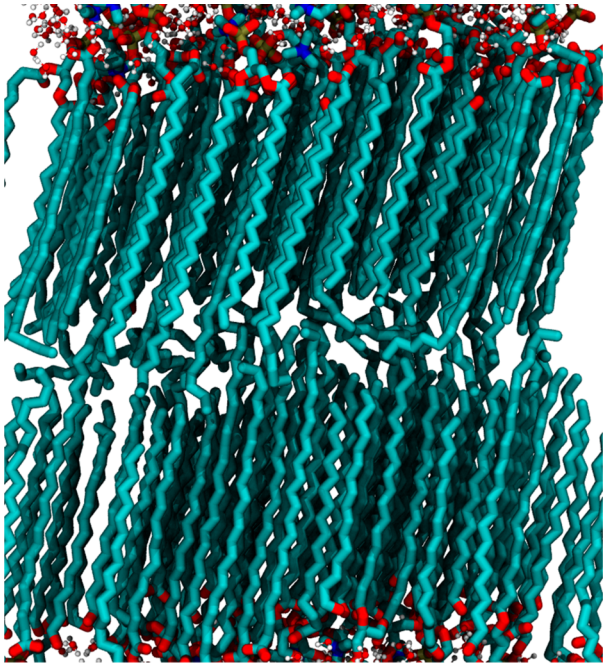

Figure 5. Simulation snapshot of 33% DSPC-OH16-FFA24 system demonstrating a lack of nematic order in the middle of the bilayer; this region predominantly contains tails of the long-tailed component, FFA24.

attributed to the noticeably longer tails in the 24-carbon components compared to the tails of the other components. Tabulated values for the offsets obtained in all of the ternary systems studied are reported in Table S2.

When looking at the effect of headgroup chemistry in the three-component systems with asymmetric tail lengths (Figure 4), the offsets are found to be similar even with slightly different headgroups. For example, when comparing DSPC-OH16-FFA12 and DSPC-OH12-FFA16 systems, the FFA12 group has a similar offset (7.44 Å for 33% DSPC) as the OH12 group (7.12 Å for 33% DSPC) and the OH16 group (5.33 Å for 33% DSPC) has a similar offset as the FFA16 group (5.16 Å or 33% DSPC).

Area per Tail (APT). The APTs of binary DSPC-OH and DSPC-FFA systems are shown in Figure 6, and the tabular data are reported in Tables S1 and S2. In general, the binary systems pack most densely when the lipid tails are of equal length (i.e., 16 carbons). For OH systems, the lipid tails appear to reach the densest packing (lowest APT) when the tails are equal in length. This suggests that the van der Waals attractions from the tail groups induces the tails to pack more tightly. However, unequal-length tails mitigate their ability to align and support other tails; longer tails cannot overlap as easily with shorter tails and result in reduced

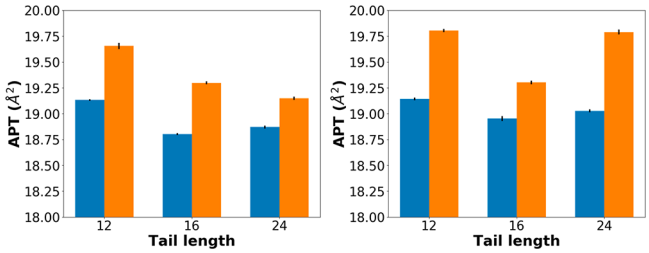

Figure 6. APT comparisons for two-component mixtures containing 33% DSPC (left) or 50% DSPC (right). Systems composed of FFA (orange) and OH (blue).

alignment and packing. For FFA systems, it is important to recognize the enlarged cross-sectional area from the FFA headgroup compared to the OH group, which introduces disorder and makes lipid packing more difficult. In the 33% DSPC−67% FFA systems, increasing the FFA tail length appears to strengthen the van der Waals attractions, overcoming the relatively larger headgroups compared to OH headgroups and increasing packing. In the 50% DSPC−50% FFA systems, increasing the number of tails relative to headgroups compared to the 33% DSPC-67% FFA systems is found to strengthen the van der Waals attractions and help overcome the enlarged headgroups. As a result, equal-length tails appear to pack the most densely (similar to the OH case).

We note that the trends seen as a function of chain length are different from those of Hartkamp et al. for the binary DSPC−alcohol mixtures.[33] In particular, in the 50%−50% DSPC−OH systems, the trends found by Hartkamp using the GROMOS force field indicate an APT minimum with the shortest tail lengths (OH12), whereas the simulations reported herein with the CHARMM force field indicate an APT minimum with OH16, i.e., the system for which the OH and DSPC chain lengths are most equal. In the 33% DSPC systems, the GROMOS simulations indicate DSPC-OH24 has a smaller APT than DSPC-OH16, while the CHARMM simulations indicate the opposite. These differences are likely due to different force field parametrizations and other subtle differences in force fields, including the use of united-atom models in GROMOS versus all-atom models in CHARMM, which may influence chain packing and tilting.[32,41] It is also important to note that the magnitude of the differences between APT values as a function of either chain length for a given force field or between force fields is still relatively small and that changes to the headgroup chemistry (i.e., either FFA or OH) are more significant.

When considering the effect of headgroup chemistry, the relative amount of DSPC is found to have a larger influence on APT compared to the lengths of the FFA or OH groups. A similar observation for the dependence of the APT on headgroup chemistry was found by Moore et al.[49] when computationally comparing ceramide-based bilayers mixed with FFAs with different tail lengths. When increasing FFA tail length, very slight APT fluctuations were found, but much larger APT variations were observed when altering the amount of FFA and ceramide content in the system.[49]

We note that the packing trends reported for gel-phase systems appear different from trends within fluid-phase systems, where 4- to 7-carbon OH components tend to increase membrane volume because short components cannot reach into the hydrophobic tail region and 8- to 12-carbon OH components tended to occupy the free volume in the tail

https://dx.doi.org/10.1021/acs.jpcb.0c00490
J. Phys. Chem. B 2020, 124, 3043−3053

region and lead to denser packing.[23] This difference can be attributed to the already dense packing of gel-phase systems versus the disordered, loose packing in fluid-phase systems.

We also note agreement with the experimental results of Hishida et al., who observed tail−tail distances (i.e., APT values) decrease with the addition of *n*-alkanes by filling in the gaps generated by the packing of large headgroups, also resulting in a more rigid structure.[21] For a pure DSPC bilayer, the simulated APT reported herein of 20.3 Å^2 drops below 20 Å^2 on mixing with single-tailed components, which agrees with the experimental observations as the addition of single-tailed components allows for closer tail spacing. However, the tail length dependence observed is not the same as that found by Hishida et al., who noted that interstitial distances between alkyl chains decreased monotonically with alkane chain length. This could be due to differences in headgroup chemistry or choice of chain lengths (Hishida et al. used 8−14 carbons; this study uses 12−24 carbons).[20,21] Additionally, the simulated DSPC APT values are in agreement with the area per chain values of 21.4 Å^2 reported by Seddon et al. from X-ray studies of DPPC bilayers.[29]

In the ternary systems (Figure 7), the introduction of a third component introduces greater offset variety that complicates

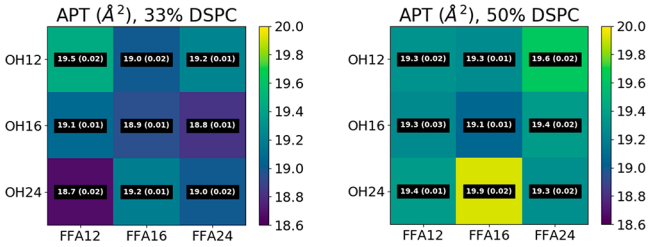

Figure 7. APT comparisons for three-component mixtures containing 33% DSPC (left) or 50% DSPC (right).

the balance of intermolecular interactions and the resultant APTs, although the general trends observed follow those found in binary systems. Furthermore, the APT values of three-component systems are generally between those of the corresponding two-component systems (i.e., 19.1, 18.8, and 19.7 Å^2 for (1:1:1) DSPC-OH16-FFA12, (1:2) DSPC-OH16, and (1:2) DSPC-FFA12, respectively).

Intrabilayer Hydrogen Bonding. Thus far, it has been shown that altering bilayer composition can result in different depth localizations (offsets) and tail packing (APT) in the binary and ternary DSPC systems studied. To examine any relationships with hydrogen-bonding networks that could arise from offset or lipid packing effects, lipid−lipid (DSPC, fatty acid, and alcohol) and lipid−water hydrogen bonding was calculated. As can be seen from the results shown in Figure 8, 33% DSPC systems appear to form a larger number of hydrogen bonds compared to 50% DSPC systems, likely due to the increased number of hydrogen bond donors (DSPC molecules have no hydrogen bond donors, only acceptors). It should be noted that hydrogen bond count trends were also consistent when looking at hydrogen bond counts normalized by available hydrogen bond donors and acceptors. Looking at headgroup chemistry effects, OH systems are found to form more hydrogen bonds compared to FFA systems, possibly due to the increased steric repulsion and disorder that mitigates the formation of hydrogen bonds in FFA systems. Similarly, longer components tend to form more hydrogen bonds compared to

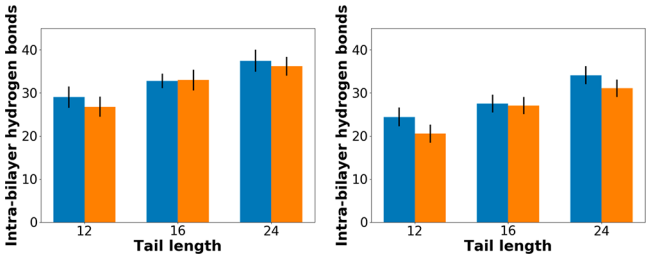

Figure 8. Lipid−lipid hydrogen bonding numbers for two-component mixtures containing 33% DSPC (left) or 50% DSPC (right). Systems are composed of FFA (orange) and OH (blue).

shorter components, which can be related to the reduced offset, i.e., closer proximity of C24 headgroups to DSPC headgroups as compared to shorter components.[77]

The calculated bilayer−water hydrogen bonding numbers are presented in Figure 9. The bilayer−water hydrogen

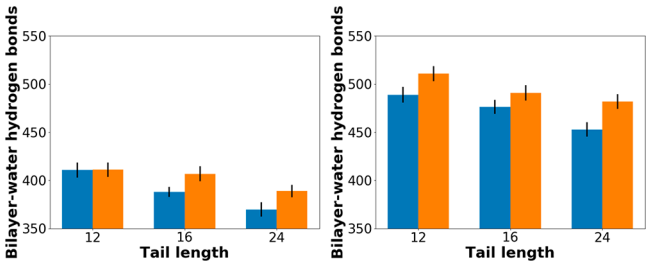

Figure 9. Lipid−water hydrogen bonding numbers for two-component mixtures containing 33% DSPC (left) or 50% DSPC (right). Systems are composed of FFA (orange) and OH (blue).

bonding trends are inversely related to the lipid−lipid hydrogen bonding—increased hydrogen bonds within the bilayer reduces the propensity for bilayer−water hydrogen bonding, and vice versa. Values for two- and three-component systems are reported in the Supporting Information. For equi-length tails, the lipid−lipid hydrogen bonding values are between those of the corresponding binary systems, i.e., (2:1:1) DSPC-OH12-FFA12, (1:1) DSPC-OH12, and (1:1) DSPC-FFA12. For asymmetric tails, the lipid−lipid hydrogen bonding values are found to be lower than that of either corresponding binary, i.e., (2:1:1) DSPC-OH16-FFA24, (1:1) DSPC-OH16, and (1:1) DSPC-FFA24, which could be due to the variegated offset effects that can prevent hydrogen bonds from forming.

Interfacial Water Relaxation. Because bilayer composition naturally appears to have an influence on the bilayer hydrogen bonding network, interfacial water dynamics may also be affected. Various groups have recognized the complex interactions between water and headgroups in phospholipid membranes, noting that water has an influence on properties including surface pressure, activity, and hydration behavior.[14,78−82] To further measure hydration behavior and interfacial water dynamics, dipole relaxation times were computed for water molecules within 1 nm of the bilayer−water interface. The dipole relaxation times for the 33% DSPC systems generally appear longer than those for 50% DSPC systems, as summarized in Figure 10. As can be seen from the data reported in Tables 2 and 3, the 33% DSPC systems have a smaller APL (tighter headgroup packing) compared to the 50% DSPC systems, and thus the more densely packed

https://dx.doi.org/10.1021/acs.jpcb.0c00490
J. Phys. Chem. B 2020, 124, 3043−3053

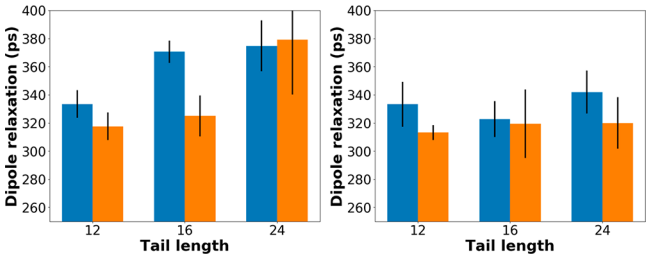

Figure 10. Water dipole relaxation times near the bilayer−water interface for two-component mixtures containing 33% DSPC (left) or 50% DSPC (right). Systems are composed of FFA (orange) and OH (blue). For reference, the corresponding pure DSPC value is about 200 ps.

hydrophilic headgroups can develop more sustained water contacts (longer dipole relaxation times) than the less densely packed 50% DSPC systems. Within the 33% DSPC systems, longer tails appear to increase the dipole relaxation times; as longer-tailed components move closer to the bilayer−water interface, the components can form more contacts with the solvent, slowing down their overall dynamics. However, for the 50% DSPC systems, the water dynamics appear dominated by the increased number of phosphocholine headgroups, masking the influence of the secondary component.

Preliminarily, the results in Figure 10 appear to contradict those of Baryiames et al., who studied heterogeneous reverse micelles and the role of composition on hydrogen bonding and interfacial water dynamics.[83] Using reverse micelles composed of sorbitan (a nonionic detergent) with FFA16-18 substitutions for hydroxyl functional groups, they observed water interfacial hydrogen bond dynamics slowed in heterogeneous (i.e., greater distribution of FFA substitutions) systems compared to homogeneous systems (i.e., no FFA substitutions) due to the ability of water to penetrate more deeply into the heterogeneous micelles. Heterogeneous systems packed poorly compared to homogeneous systems, creating space for water penetration and thus slower dynamics. In contrast, our systems demonstrate greater packing when heterogeneous; the ability for the lipids to offset their position within the bilayer creates space for greater water penetration, resulting in slower water dynamics compared to pure DSPC. However, although shorter components with deeper offsets in our bilayers can yield greater water penetration and possibly slower water dynamics, the reduction in solvent−headgroup contact accelerates water dynamics. Rationalizing the results obtained with Baryiames' findings, it appears 24-carbon components and their offsets provide a balance of solvent−headgroup contact and water penetration that results in slower water dynamics compared to shorter length components.

In summary, generally, OH components appear to slow down interfacial water more than FFA components due to less offset promoting more solvent contact with DSPC headgroups. Longer components also appear to slow down interfacial water. The results for ternary systems follow similar trends and are presented in the Supporting Information (Tables S1 and S2). The dipole relaxation times of three-component systems are typically found to be between the corresponding two-component systems (i.e., (2:1:1) DSPC-OH16-FFA12 has a dipole relaxation time between (1:1) DSPC-OH16 and (1:1) DSPC-FFA12).

Area per Lipid (APL). Tables 2 and 3 report several additional structural metrics for the bilayer systems studied, including the APL. In general, the APL is found to be mostly dependent on the DSPC fraction. Given the size of the DSPC headgroup and the fact that DSPC has two tails compared to the other lipids, this is not surprising and consistent with results found in earlier work.[33] FFA molecules tend to increase the APL more than OH molecules, similarly due to slightly increased steric repulsions. At 33% DSPC, the APL remains fairly constant with changes in tail length, which could be due to the prevalence of smaller headgroups (by substituting DSPC with FFA or OH), resulting in less steric repulsion and more muted effects on APL. At 50% DSPC, where the DSPC headgroups are more prevalent and can emphasize effects on APL, the APL slightly increases with tail length, which can be attributed to the reduced component offset (see Figures 3 and 4) and closer proximity between different components (see offset discussion earlier). For example, 24-carbon length tails move closer to the bilayer−water interface, introduce greater steric repulsions to the DSPC headgroups, and cause the headgroups to laterally spread apart. We note similar results

Table 2. Area per Lipid (APL), Bilayer Height, Interdigitation (I_{dig}), *S2*, and Tilt Values for Pure DSPC and 33% DSPC Systems

system	APL (Å^2)	height (Å)	I_{dig} (Å)	nematic order (*S2*)	tilt (deg)
DSPC	50.4 (0.1)	46.6 (0.1)	3.06 (0.04)	0.964 (0.001)	35.9 (0.2)
(1:2) DSPC-FFA12	26.79 (0.05)	49.79 (0.06)	3.72 (0.03)	0.9715 (0.0008)	11.2 (0.4)
(1:2) DSPC-FFA16	26.89 (0.06)	52.45 (0.11)	2.78 (0.01)	0.9801 (0.0005)	16.4 (0.5)
(1:2) DSPC-FFA24	27.18 (0.08)	60.51 (0.18)	5.98 (0.01)	0.9818 (0.0004)	18.5 (0.5)
(1:2) DSPC-OH12	25.98 (0.01)	49.95 (0.06)	3.48 (0.01)	0.9813 (0.0003)	10.0 (0.2)
(1:2) DSPC-OH16	25.41 (0.03)	54.25 (0.06)	2.02 (0.01)	0.9882 (0.0002)	9.1 (0.3)
(1:2) DSPC-OH24	26.44 (0.04)	61.23 (0.10)	6.06 (0.01)	0.9842 (0.0003)	15.0 (0.3)
(1:1:1) DSPC-OH12-FFA12	26.76 (0.03)	49.84 (0.08)	3.36 (0.06)	0.9778 (0.0006)	10.5 (0.2)
(1:1:1) DSPC-OH12-FFA16	26.42 (0.07)	51.75 (0.11)	2.66 (0.06)	0.9832 (0.0002)	13.1 (0.4)
(1:1:1) DSPC-OH12-FFA24	26.95 (0.03)	55.77 (0.09)	6.55 (0.13)	0.9753 (0.0005)	13.4 (0.2)
(1:1:1) DSPC-OH16-FFA12	26.33 (0.05)	52.21 (0.06)	2.99 (0.04)	0.9829 (0.0004)	11.1 (0.4)
(1:1:1) DSPC-OH16-FFA16	26.45 (0.10)	53.53 (0.18)	2.56 (0.04)	0.9861 (0.0004)	13.5 (0.9)
(1:1:1) DSPC-OH16-FFA24	26.38 (0.14)	57.98 (0.25)	5.23 (0.13)	0.9831 (0.0007)	14.6 (0.8)
(1:1:1) DSPC-OH24-FFA12	25.59 (0.05)	58.30 (0.07)	7.63 (0.20)	0.9775 (0.0005)	10.2 (0.5)
(1:1:1) DSPC-OH24-FFA16	27.20 (0.06)	56.73 (0.11)	5.94 (0.14)	0.9796 (0.0004)	15.0 (0.4)
(1:1:1) DSPC-OH24-FFA24	26.77 (0.08)	61.57 (0.14)	6.74 (0.12)	0.9833 (0.0004)	15.9 (0.6)

https://dx.doi.org/10.1021/acs.jpcb.0c00490
J. Phys. Chem. B 2020, 124, 3043−3053

Table 3. Area per Lipid (APL), Height, Interdigitation (I_{dig}), *S*2, and Tilt Values for 50% DSPC Systems

system	APL (Å^2)	height (Å)	I_{dig} (Å)	nematic order (*S*2)	tilt (deg)
(1:1) DSPC-FFA12	30.78 (0.04)	51.33 (0.08)	3.55 (0.07)	0.9675 (0.0009)	13.1 (0.3)
(1:1) DSPC-FFA16	30.95 (0.09)	52.66 (0.10)	3.13 (0.13)	0.9802 (0.0005)	19.5 (0.4)
(1:1) DSPC-FFA24	32.13 (0.12)	56.87 (0.18)	6.98 (0.13)	0.9631 (0.0013)	21.2 (0.6)
(1:1) DSPC-OH12	29.33 (0.05)	52.49 (0.04)	2.89 (0.08)	0.9816 (0.0002)	9.9 (0.4)
(1:1) DSPC-OH16	29.94 (0.07)	53.59 (0.11)	2.43 (0.08)	0.9828 (0.0002)	16.9 (0.5)
(1:1) DSPC-OH24	30.86 (0.06)	58.09 (0.13)	6.58 (0.10)	0.9778 (0.0006)	19.6 (0.5)
(2:1:1) DSPC-OH12-FFA12	29.99 (0.08)	51.74 (0.09)	3.44 (0.16)	0.9746 (0.0007)	13.4 (0.5)
(2:1:1) DSPC-OH12-FFA16	30.13 (0.08)	52.56 (0.14)	2.99 (0.13)	0.9780 (0.0003)	14.6 (0.6)
(2:1:1) DSPC-OH12-FFA24	30.80 (0.10)	54.88 (0.15)	5.95 (0.11)	0.9653 (0.0011)	15.6 (0.5)
(2:1:1) DSPC-OH16-FFA12	30.33 (0.08)	52.48 (0.12)	3.06 (0.01)	0.9794 (0.0007)	16.0 (0.7)
(2:1:1) DSPC-OH16-FFA16	29.93 (0.13)	53.88 (0.17)	2.76 (0.01)	0.9847 (0.0004)	16.6 (0.7)
(2:1:1) DSPC-OH16-FFA24	30.35 (0.11)	56.40 (0.21)	6.14 (0.14)	0.9781 (0.0006)	15.6 (0.7)
(2:1:1) DSPC-OH24-FFA12	29.79 (0.09)	56.43 (0.17)	7.14 (0.19)	0.9729 (0.0015)	11.2 (0.7)
(2:1:1) DSPC-OH24-FFA16	31.55 (0.08)	54.90 (0.09)	7.13 (0.09)	0.9655 (0.0015)	17.3 (0.5)
(2:1:1) DSPC-OH24-FFA24	31.12 (0.08)	58.14 (0.16)	6.50 (0.10)	0.9757 (0.0008)	20.1 (0.5)

were obtained by Hishida et al., who found that alkanes increase the head−head distance in 70 mol % DMPC bilayers with 30 mol % alkane (8- to 14-carbon tails).[21]

Chain Tilt Angle. Tilt angle (Tables 2 and 3) appears to be dependent on both DSPC fraction and tail length. While larger headgroups induce greater steric repulsion that pushes the lipids apart and increases APL, tilting provides the lipid tails with a mechanism to maximize van der Waals interactions while reducing steric repulsions. Furthermore, longer tails enhance the strength of the van der Waals interaction, resulting in a larger tilt angle. Again the values reported in Tables 2 and 3 are similar to that observed by Hartkamp et al.[33] Additionally, the results are consistent with the work of Seddon et al., who reported that the addition of FFA reduces the tilt of gel-phase bilayers.[29,45] It should be noted that our 33% DSPC−67% FFA mixtures not only demonstrate a low tilt angle but also a low APL. This could indicate an already-favorable distribution of lipids along the bilayer normal without needing to tilt or laterally spread out compared to other DSPC−FFA mixtures that require tilting to obtain a favorable configuration.

Bilayer Height, Chain Interdigitation (I_{dig}), and *S*2. Bilayer height generally increases with the tail length as longer tails naturally increase the thickness of each leaflet. Bilayer heights are, however, also affected by tilt angles and interdigitation. Compared to FFA components, OH components generally result in taller bilayers due to the lower tilt angles. At 33% DSPC, the 12- and 24-carbon FFA and OH bilayers display the same height due to the interdigitation and tilt angle properties balancing each other out. Interdigitation measures the amount of leaflet−leaflet overlap, with greater interdigitation values indicating higher leaflet−leaflet overlap. The amount of interdigitation is found to depend on the amount of tail-length asymmetry, similar to earlier work.[33] DSPC tails are 18 carbons long, which effectively reach to similar depths as OH16 and FFA16 when considering component offset. Because of this similarity in tail length, there is little room for opposing leaflets to interdigitate. By shortening or lengthening one component, the resulting tail-length asymmetry creates space for the opposing leaflet. A similar observation was found by Aagaard et al., who reported a "mismatch effect" that had influence on molar volume.[23]

CONCLUSION

Two- and three-component gel-phase DSPC-based lipid bilayers were studied with compositions that included DSPC and combinations of OH and FFA with 12-, 16-, and 24-carbon tails. We observe that headgroup repulsion and tail-length asymmetry drive shorter components deeper within the bilayer. These component offsets influence tail alignment and tail packing (APT). Furthermore, the component offsets and APT properties affect lipid−lipid hydrogen bonding; tighter-packed tails and greater lipid−lipid hydrogen bonding appear correlated. As a result of tail packing and lipid−lipid hydrogen bond networks, the interfacial solvent dynamics are impacted, as observed by water dipole relaxation times.

Bilayer structure is found to be largely dictated by steric repulsions from headgroups and van der Waals attractions from tails. Larger headgroups create greater steric repulsion, and longer tails provide greater van der Waals attraction. By modifying headgroups and chain length (altering chemical composition), the structure of gel-phase bilayers can be tuned. OH and FFA components possess chemically similar tails but different headgroups, which has small effects on resultant bilayer properties. Shorter-tailed components are found deeper within the bilayer, which can help mitigate the steric repulsions at the bilayer−water interface but reduces the amount of lipid−lipid hydrogen bonding. Generally, APL and tilt angle are observed to be most affected by DSPC fraction, although secondary and tertiary components can introduce offsets that can slightly modify the steric repulsions. Bilayer height is seen to be naturally most strongly connected to tail length but also influenced by the tilt angle. The area per tail and nematic order depend on headgroup size and tail length, but OH components and 16-carbon tails generally exhibit the lowest APT and highest *S*2. Interdigitation is most affected by tail length asymmetry. Dipole relaxation times of interfacial water appear dependent on the area per lipid due to the ability of hydrophilic headgroups to form contacts with water.

The three-component systems examined in this study demonstrate many of the same structural trends (across all reported properties) as the two-component systems, namely dependence on DSPC fraction and tail length with some modest differences when mixing OH and FFA headgroups. By increasing the variety of tail lengths in the system, components can displace themselves depthwise and provide an additional mechanism for generating stable, tightly packed, configura-

https://dx.doi.org/10.1021/acs.jpcb.0c00490
J. Phys. Chem. B 2020, 124, 3043−3053

tions. The DSPC fractions studied are the same as those examined in the two-component systems (33% and 50%), but the non-DSPC component in the two-component system can be viewed as having been partially substituted with a third component, further altering tail length or headgroup chemistry. Results for three-component systems follow similar trends as two-component systems and can be found in the Supporting Information.

Overall, these results shed light on the mechanisms by which lipids can pack differently in gel-phase bilayers. By understanding how the composition of headgroups and tail lengths affects the balance between steric repulsion and van der Waals attraction, formulations can be designed with particular structures in mind. In addition, this may shed light on how composition can be used to tune the barrier properties of gel-phase membranes, including the use of smaller head groups and tail length symmetry to yield tight lipid packing and potentially prohibit solute permeation.

■ ASSOCIATED CONTENT

Supporting Information

The Supporting Information is available free of charge at https://pubs.acs.org/doi/10.1021/acs.jpcb.0c00490.

Links to GitHub repositories containing scripts, simulations, and force field details; supplemental bilayer analysis (PDF)

■ AUTHOR INFORMATION

Corresponding Author

Clare McCabe − *Department of Chemical and Biomolecular Engineering, Multiscale Modeling and Simulation Center, and Department of Chemistry, Vanderbilt University, Nashville, Tennessee 37212, United States;* orcid.org/0000-0002-8552-9135; Email: c.mccabe@vanderbilt.edu

Authors

Alexander Yang − *Department of Chemical and Biomolecular Engineering and Multiscale Modeling and Simulation Center, Vanderbilt University, Nashville, Tennessee 37212, United States;* orcid.org/0000-0002-3678-0075

Timothy C. Moore − *Department of Chemical and Biomolecular Engineering and Multiscale Modeling and Simulation Center, Vanderbilt University, Nashville, Tennessee 37212, United States*

Christopher R. Iacovella − *Department of Chemical and Biomolecular Engineering and Multiscale Modeling and Simulation Center, Vanderbilt University, Nashville, Tennessee 37212, United States;* orcid.org/0000-0003-0557-0427

Michael Thompson − *GlaxoSmithKline Consumer Health Care, Warren, New Jersey 07059, United States*

David J. Moore − *GlaxoSmithKline Consumer Health Care, Warren, New Jersey 07059, United States*

Complete contact information is available at: https://pubs.acs.org/10.1021/acs.jpcb.0c00490

Notes

The authors declare no competing financial interest.

■ ACKNOWLEDGMENTS

Computational resources were provided by the National Energy Research Scientific Computing Center, supported by the Office of Science of the Department of Energy under Contract DE-AC02-05CH11231. This work was conducted in part using the resources of the Advanced Computing Center for Research and Education at Vanderbilt University. CMC and CRI acknowledge partial support from the National Institute of Arthritis and Musculoskeletal and Skin Diseases grant R01AR07267.

■ REFERENCES

(1) Pilgram, G. S. K.; Vissers, D. C. J.; Van Der Meulen, H.; Pavel, S.; Lavrijsen, S. P. M.; Bouwstra, J. A.; Koerten, H. K. Aberrant Lipid Organization in Stratum Corneum of Patients with Atopic Dermatitis and Lamellar Ichthyosis. *J. Invest. Dermatol.* **2001**, *117* (3), 710−717.

(2) Van Smeden, J.; Janssens, M.; Gooris, G. S.; Bouwstra, J. A. The Important Role of Stratum Corneum Lipids for the Cutaneous Barrier Function. *Biochim. Biophys. Acta, Mol. Cell Biol. Lipids* **2014**, *1841* (3), 295−313.

(3) Caussin, J.; Gooris, G. S.; Bouwstra, J. A. FTIR Studies Show Lipophilic Moisturizers to Interact with Stratum Corneum Lipids, Rendering the More Densely Packed. *Biochim. Biophys. Acta, Biomembr.* **2008**, *1778* (6), 1517−1524.

(4) Groen, D.; Poole, D. S.; Gooris, G. S.; Bouwstra, J. A. Is an Orthorhombic Lateral Packing and a Proper Lamellar Organization Important for the Skin Barrier Function? *Biochim. Biophys. Acta, Biomembr.* **2011**, *1808* (6), 1529−1537.

(5) Tardieu, A.; Luzzati, V.; Reman, F. C. Structure and Polymorphism of the Hydrocarbon Chains of Lipids: A Study of Lecithin-Water Phases. *J. Mol. Biol.* **1973**, *75* (4), 711−733.

(6) Caussin, J.; Gooris, G. S.; Groenink, H. W. W.; Wiechers, J. W.; Bouwstra, J. A. Interaction of Lipophilic Moisturizers on Stratum Corneum Lipid Domains in Vitro and in Vivo. *Skin Pharmacol. Physiol.* **2007**, *20* (4), 175−186.

(7) Gooris, G. S.; Kamran, M.; Kros, A.; Moore, D. J.; Bouwstra, J. A. Interactions of Dipalmitoylphosphatidylcholine with Ceramide-Based Mixtures. *Biochim. Biophys. Acta, Biomembr.* **2018**, *1860* (6), 1272−1281.

(8) Pennick, G.; Chavan, B.; Summers, B.; Rawlings, A. V. The Effect of an Amphiphilic Self-Assembled Lipid Lamellar Phase on the Relief of Dry Skin. *Int. J. Cosmet. Sci.* **2012**, *34* (6), 567−574.

(9) Pennick, G.; Harrison, S.; Jones, D.; Rawlings, A. V. Superior Effect of Isostearyl Isostearate on Improvement in Stratum Corneum Water Permeability Barrier Function as Examined by the Plastic Occlusion Stress Test. *Int. J. Cosmet. Sci.* **2010**, *32* (4), 304−312.

(10) Summers, R. S.; Summers, B.; Chandar, P.; Feinberg, C.; Gursky, R.; Rawlings, A. V. The Effect of Lipids, with and without Humectant, on Skin Xerosis. *J. Soc. Cosmet. Chem.* **1996**, *47* (February), 27−39.

(11) Bulsara, P. A.; Varlashkin, P.; Dickens, J.; Moore, D. J.; Rawlings, A. V.; Clarke, M. J. The Rational Design of Biomimetic Skin Barrier Lipid Formulations Using Biophysical Methods. *Int. J. Cosmet. Sci.* **2017**, *39* (2), 206−216.

(12) Lis, L. J.; McAlister, M.; Fuller, N.; Rand, R. P.; Parsegian, V. A. Interactions between Neutral Phospholipid Bilayer Membranes. *Biophys. J.* **1982**, *37* (3), 657−665.

(13) Rand, R. P.; Parsegian, V. A. Hydration Forces between Phospholipid Bilayers. *Biochim. Biophys. Acta, Rev. Biomembr.* **1989**, *988* (3), 351−376.

(14) Smith, G. S.; Sirota, E. B.; Safinya, C. R.; Plano, R. J.; Clark, N. A. X-Ray Structural Studies of Freely Suspended Ordered Hydrated DMPC Multimembrane Films. *J. Chem. Phys.* **1990**, *92* (7), 4519−4529.

(15) Nagle, J. F.; Cognet, P.; Dupuy, F. G.; Tristram-Nagle, S. Structure of Gel Phase DPPC Determined by X-Ray Diffraction. *Chem. Phys. Lipids* **2019**, *218* (6), 168−177.

(16) Sun, W. J.; Tristram-Nagle, S.; Suter, R. M.; Nagle, J. F. Structure of Gel Phase Saturated Lecithin Bilayers: Temperature and Chain Length Dependence. *Biophys. J.* **1996**, *71* (2), 885−891.

(17) Tristram-Nagle, S.; Zhang, R.; Suter, R. M.; Worthington, C. R.; Sun, W. J.; Nagle, J. F. Measurement of Chain Tilt Angle in Fully

Hydrated Bilayers of Gel Phase Lecithins. *Biophys. J.* **1993**, *64* (4), 1097−1109.
(18) Wiener, M. C.; Suter, R. M.; Nagle, J. F. Structure of the Fully Hydrated Gel Phase of Dipalmitoylphosphatidylcholine. *Biophys. J.* **1989**, *55* (2), 315−325.
(19) Akabori, K.; Nagle, J. F. Structure of the DMPC Lipid Bilayer Ripple Phase. *Soft Matter* **2015**, *11* (5), 918−926.
(20) Hishida, M.; Yanagisawa, R.; Yamamura, Y.; Saito, K. Phase Separation of a Ternary Lipid Vesicle Including *n* -Alkane: Rugged Vesicle and Bilayer Flakes Formed by Separation between Highly Rigid and Flexible Domains. *J. Chem. Phys.* **2019**, *150* (6), 064904.
(21) Hishida, M.; Endo, A.; Nakazawa, K.; Yamamura, Y.; Saito, K. Effect of N-Alkanes on Lipid Bilayers Depending on Headgroups. *Chem. Phys. Lipids* **2015**, *188*, 61−67.
(22) Hishida, M.; Yanagisawa, R.; Usuda, H.; Yamamura, Y.; Saito, K. Communication: Rigidification of a Lipid Bilayer by an Incorporated n -Alkane. *J. Chem. Phys.* **2016**, *144* (4), 041103.
(23) Aagaard, T. H.; Kristensen, M. N.; Westh, P. Packing Properties of 1-Alkanols and Alkanes in a Phospholipid Membrane. *Biophys. Chem.* **2006**, *119* (1), 61−68.
(24) Ingólfsson, H. I.; Andersen, O. S. Alcohol's Effects on Lipid Bilayer Properties. *Biophys. J.* **2011**, *101* (4), 847−855.
(25) Lyon, R. C.; McComb, J. A.; Schreurs, J.; Goldstein, D. B. A Relationship between Alcohol Intoxication and the Disordering of Brain Membranes by a Series of Short-Chain Alcohols. *J. Pharmacol. Exp. Ther.* **1981**, *218* (3), 669−675.
(26) Ly, H. V.; Longo, M. L. The Influence of Short-Chain Alcohols on Interfacial Tension, Mechanical Properties, Area/Molecule, and Permeability of Fluid Lipid Bilayers. *Biophys. J.* **2004**, *87* (2), 1013−1033.
(27) Falck, E.; Patra, M.; Karttunen, M.; Hyvönen, M. T.; Vattulainen, I. Lessons of Slicing Membranes: Interplay of Packing, Free Area, and Lateral Diffusion in Phospholipid/Cholesterol Bilayers. *Biophys. J.* **2004**, *87* (2), 1076−1091.
(28) Ma, Y.; Ghosh, S. K.; Dilena, D. A.; Bera, S.; Lurio, L. B.; Parikh, A. N.; Sinha, S. K. Cholesterol Partition and Condensing Effect in Phase-Separated Ternary Mixture Lipid Multilayers. *Biophys. J.* **2016**, *110* (6), 1355−1366.
(29) Seddon, J. M.; Templer, R. H.; Warrender, N. A.; Huang, Z.; Cevc, G.; Marsh, D. Phosphatidylcholine−Fatty Acid Membranes: Effects of Headgroup Hydration on the Phase Behaviour and Structural Parameters of the Gel and Inverse Hexagonal (HII) Phases. *Biochim. Biophys. Acta, Biomembr.* **1997**, *1327* (1), 131−147.
(30) Tu, K.; Tobias, D. J.; Blasie, J. K.; Klein, M. L. Molecular Dynamics Investigation of the Structure of a Fully Hydrated Gel-Phase Dipalmitoylphosphatidylcholine Bilayer. *Biophys. J.* **1996**, *70* (2), 595−608.
(31) Essmann, U.; Perera, L.; Berkowitz, M. L. The Origin of the Hydration Interaction of Lipid Bilayers from MD Simulation of Dipalmitoylphosphatidylcholine Membranes in Gel and Liquid Crystalline Phases. *Langmuir* **1995**, *11* (24), 4519−4531.
(32) Poger, D.; van Gunsteren, W. F.; Mark, A. E. A New Force Field for Simulating Phosphatidylcholine Bilayers. *J. Comput. Chem.* **2010**, *31* (6), 1117−1125.
(33) Hartkamp, R.; Moore, T. C.; Iacovella, C. R.; Thompson, M. A.; Bulsara, P. A.; Moore, D. J.; M^{c}Cabe, C. Structural Properties of Phospholipid-Based Bilayers with Long- Chain Alcohol Molecules in the Gel Phase. *J. Phys. Chem. B* **2016**, *120* (50), 12863−12871.
(34) Hartkamp, R.; Moore, T. C.; Iacovella, C. R.; Thompson, M. A.; Bulsara, P. A.; Moore, D. J.; M^{c}Cabe, C. Investigating the Structure of Multicomponent Gel-Phase Lipid Bilayers. *Biophys. J.* **2016**, *111* (4), 813−823.
(35) Hartkamp, R.; Moore, T. C.; Iacovella, C. R.; Thompson, M. A.; Bulsara, P. A.; Moore, D. J.; M^{c}Cabe, C. Composition Dependence of Water Permeation Across Multicomponent Gel-Phase Bilayers. *J. Phys. Chem. B* **2018**, *122* (12), 3113−3123.
(36) Venable, R. M.; Brooks, B. R.; Pastor, R. W. Molecular Dynamics Simulations of Gel (LβI) Phase Lipid Bilayers in Constant Pressure and Constant Surface Area Ensembles. *J. Chem. Phys.* **2000**, *112* (10), 4822−4832.
(37) Feller, S. E.; Pastor, R. W. Constant Surface Tension Simulations of Lipid Bilayers: The Sensitivity of Surface Areas and Compressibilities. *J. Chem. Phys.* **1999**, *111* (3), 1281−1287.
(38) Klauda, J. B.; Brooks, B. R.; Pastor, R. W. Dynamical Motions of Lipids and a Finite Size Effect in Simulations of Bilayers. *J. Chem. Phys.* **2006**, *125* (14), 144710.
(39) Leonard, A. N.; Pastor, R. W.; Klauda, B. Parameterization of the CHARMM All-Atom Force Field for Ether Lipids and Model Linear Ethers, 2018.
(40) Leonard, A. N.; Wang, E.; Monje-Galvan, V.; Klauda, J. B. Developing and Testing of Lipid Force Fields with Applications to Modeling Cellular Membranes. *Chem. Rev.* **2019**, *119* (9), 6227−6269.
(41) Klauda, J. B.; Venable, R. M.; Freites, J. A.; O'Connor, J. W.; Tobias, D. J.; Mondragon-Ramirez, C.; Vorobyov, I.; MacKerell, A. D., Jr.; Pastor, R. W. Update of the CHARMM All-Atom Additive Force Field for Lipids: Validation on Six Lipid Types. *J. Phys. Chem. B* **2010**, *114* (23), 7830−7843.
(42) Klauda, J. B.; Kučerka, N.; Brooks, B. R.; Pastor, R. W.; Nagle, J. F. Simulation-Based Methods for Interpreting x-Ray Data from Lipid Bilayers. *Biophys. J.* **2006**, *90* (8), 2796−2807.
(43) Pastor, R. W.; MacKerell, A. D. Development of the CHARMM Force Field for Lipids. *J. Phys. Chem. Lett.* **2011**, *2* (13), 1526−1532.
(44) Boughter, C. T.; Monje-Galvan, V.; Im, W.; Klauda, J. B. Influence of Cholesterol on Phospholipid Bilayer Structure and Dynamics. *J. Phys. Chem. B* **2016**, *120*, 11761.
(45) Khakbaz, P.; Klauda, J. B. Investigation of Phase Transitions of Saturated Phosphocholine Lipid Bilayers via Molecular Dynamics Simulations. *Biochim. Biophys. Acta, Biomembr.* **2018**, *1860* (April), 1489−1501.
(46) Ermilova, I.; Lyubartsev, A. P. Cholesterol in Phospholipid Bilayers: Positions and Orientations inside Membranes with Different Unsaturation Degrees. *Soft Matter* **2019**, *15* (1), 78−93.
(47) Klein, C.; Sallai, J.; Jones, T. J.; Iacovella, C. R.; M^{c}Cabe, C.; Cummings, P. T. A Hierarchical, Component Based Approach to Screening Properties of Soft Matter. In *Foundations of Molecular Modeling and Simulation: Select Papers from FOMMS 2015*; Snurr, R. Q., Adjiman, C. S., Kofke, D. A., Eds.; Springer: Singapore, 2016; pp 79−92.
(48) Uppulury, K.; Coppock, P. S.; Kindt, J. T. Molecular Simulation of the DPPE Lipid Bilayer Gel Phase: Coupling between Molecular Packing Order and Tail Tilt Angle. *J. Phys. Chem. B* **2015**, *119* (28), 8725−8733.
(49) Moore, T. C.; Hartkamp, R.; Iacovella, C. R.; Bunge, A. L.; M^{c}Cabe, C. Effect of Ceramide Tail Length on the Structure of Model Stratum Corneum Lipid Bilayers. *Biophys. J.* **2018**, *114* (1), 113−125.
(50) Lindahl, E.; Hess, B.; van der Spoel, D. GROMACS 3.0: A Package for Molecular Simulation and Trajectory Analysis. *J. Mol. Model.* **2001**, *7* (8), 306−317.
(51) Hess, B.; Kutzner, C.; van der Spoel, D.; Lindahl, E. GROMACS 4: Algorithms for Highly Efficient, Load-Balanced, and Scalable Molecular Simulation. *J. Chem. Theory Comput.* **2008**, *4* (3), 435−447.
(52) Berendsen, H. J. C.; van der Spoel, D.; van Drunen, R. GROMACS: A Message-Passing Parallel Molecular Dynamics Implementation. *Comput. Phys. Commun.* **1995**, *91* (1), 43−56.
(53) Páll, S.; Abraham, M. J.; Kutzner, C.; Hess, B.; Lindahl, E. Tackling Exascale Software Challenges in Molecular Dynamics Simulations with GROMACS. In *Solving Software Challenges for Exascale: International Conference on Exascale Applications and Software, EASC 2014, Stockholm, Sweden*, April 2−3, 2014, Revised Selected Papers; Markidis, S., Laure, E., Eds.; Springer International Publishing: Cham, 2015; pp 3−27.
(54) Van Der Spoel, D.; Lindahl, E.; Hess, B.; Groenhof, G.; Mark, A. E.; Berendsen, H. J. C. GROMACS: Fast, Flexible, and Free. *J. Comput. Chem.* **2005**, *26* (16), 1701−1718.

https://dx.doi.org/10.1021/acs.jpcb.0c00490
J. Phys. Chem. B 2020, 124, 3043−3053

(55) Pronk, S.; Pall, S.; Schulz, R.; Larsson, P.; Bjelkmar, P.; Apostolov, R.; Shirts, M. R.; Smith, J. C.; Kasson, P. M.; van der Spoel, D.; et al. GROMACS 4.5: A High-Throughput and Highly Parallel Open Source Molecular Simulation Toolkit. *Bioinformatics* **2013**, *29* (7), 845.
(56) Abraham, M. J.; Murtola, T.; Schulz, R.; Pall, S.; Smith, J. C.; Hess, B.; Lindahl, E. GROMACS: High Performance Molecular Simulations through Multi-Level Parallelism from Laptops to Supercomputers. *SoftwareX* **2015**, *1−2*, 19−25.
(57) Jo, S.; Kim, T.; Iyer, V.; Im, W. CHARMM-GUI: A Web-Based Graphical User Interface for CHARMM. *J. Comput. Chem.* **2008**, *29*, 1859−1865.
(58) Klauda, J. B.; Venable, R. M.; et al. Update of the CHARMM All-Atom Additive Force Field for Lipids: Validation on Six Lipid Types. *J. Phys. Chem. B* **2010**, *114*, 7830.
(59) Jorgensen, W. L.; Chandrasekhar, J.; Madura, J. D.; Impey, R. W.; Klein, M. L. Comparison of Simple Potential Functions for Simulating Liquid Water. *J. Chem. Phys.* **1983**, *79* (2), 926−935.
(60) Miyamoto, S.; Kollman, P. A. Settle: An Analytical Version of the SHAKE and RATTLE Algorithm for Rigid Water Models. *J. Comput. Chem.* **1992**, *13* (8), 952−962.
(61) MacKerell, A. D.; Bashford, D.; Bellott, M.; Dunbrack, R. L.; Evanseck, J. D.; Field, M. J.; Fischer, S.; Gao, J.; Guo, H.; Ha, S.; et al. All-Atom Empirical Potential for Molecular Modeling and Dynamics Studies of Proteins. *J. Phys. Chem. B* **1998**, *102* (18), 3586−3616.
(62) Hess, B. P-LINCS: A Parallel Linear Constraint Solver for Molecular Simulation. *J. Chem. Theory Comput.* **2008**, *4* (1), 116−122.
(63) Essmann, U.; Perera, L.; Berkowitz, M. L.; Darden, T.; Lee, H.; Pedersen, L. G. A Smooth Particle Mesh Ewald Method. *J. Chem. Phys.* **1995**, *103* (19), 8577−8593.
(64) Nosé, S. A Unified Formulation of the Constant Temperature Molecular Dynamics Methods. *J. Chem. Phys.* **1984**, *81* (1), 511−519.
(65) Hoover, W. G. Canonical Dynamics: Equilibrium Phase-Space Distributions. *Phys. Rev. A: At., Mol., Opt. Phys.* **1985**, *31* (3), 1695−1697.
(66) Parrinello, M.; Rahman, A. Polymorphic Transitions in Single Crystals: A New Molecular Dynamics Method. *J. Appl. Phys.* **1981**, *52* (12), 7182−7190.
(67) Mabrey, S.; Sturtevant, J. M. Investigation of Phase Transitions of Lipids and Lipid Mixtures by High Sensitivity Differential Scanning Calorimetry. *Proc. Natl. Acad. Sci. U. S. A.* **1976**, *73* (11), 3862−3866.
(68) Wilson, M. R. Determination of Order Parameters in Realistic Atom-Based Models of Liquid Crystal Systems. *J. Mol. Liq.* **1996**, *68* (1), 23−31.
(69) Guo, S.; Moore, T. C.; Iacovella, C. R.; Strickland, L. A.; M^{c}Cabe, C. Simulation Study of the Structure and Phase Behavior of Ceramide Bilayers and the Role of Lipid Headgroup Chemistry. *J. Chem. Theory Comput.* **2013**, *9* (11), 5116−5126.
(70) McGibbon, R. T.; Beauchamp, K. A.; Harrigan, M. P.; Klein, C.; Swails, J. M.; Hernández, C. X.; Schwantes, C. R.; Wang, L. P.; Lane, T. J.; Pande, V. S. MDTraj: A Modern Open Library for the Analysis of Molecular Dynamics Trajectories. *Biophys. J.* **2015**, *109* (8), 1528−1532.
(71) Gowers, R.; Linke, M.; Barnoud, J.; Reddy, T.; Melo, M.; Seyler, S.; Domański, J.; Dotson, D.; Buchoux, S.; Kenney, I.; et al. MDAnalysis: A Python Package for the Rapid Analysis of Molecular Dynamics Simulations. In *Proceedings of the 15th Python in Science Conference*; 2016; pp 98−105.
(72) Michaud-Agrawal, N.; Denning, E. J.; Woolf, T. B.; Beckstein, O. MDAnalysis: A Toolkit for the Analysis of Molecular Dynamics Simulations. *J. Comput. Chem.* **2011**, *32*, 2319−2327.
(73) Jones, E.; Oliphant, T.; Peterson, P. SciPy: Open source scientific tools for Python.
(74) Van Der Walt, S.; Colbert, S. C.; Varoquaux, G. The NumPy Array: A Structure for Efficient Numerical Computation. *Comput. Sci. Eng.* **2011**, *13* (2), 22−30.
(75) McKinney, W. Data Structures for Statistical Computing in Python. *Proc. 9th Python Sci. Conf.* **2010**, 51−56.
(76) Hunter, J. D. Matplotlib: A 2D Graphics Environment. *Comput. Sci. Eng.* **2007**, *9* (3), 90−95.
(77) Wang, E.; Klauda, J. B. Simulations of Pure Ceramide and Ternary Lipid Mixtures as Simple Interior Stratum Corneum Models. *J. Phys. Chem. B* **2018**, *122*, 11996.
(78) Disalvo, E. A.; Pinto, O. A.; Martini, M. F.; Bouchet, A. M.; Hollmann, A.; Frías, M. A. Functional Role of Water in Membranes Updated: A Tribute to Träuble. *Biochim. Biophys. Acta, Biomembr.* **2015**, *1848* (7), 1552−1562.
(79) Katsaras, J.; Raghunathan, V. A.; Dufourc, E. J.; Dufourcq, J. Evidence for a Two-Dimensional Molecular Lattice in Subgel Phase DPPC Bilayers. *Biochemistry* **1995**, *34* (14), 4684−4688.
(80) Mason, P. C.; Gaulin, B. D.; Epand, R. M.; Katsaras, J. Critical Swelling in Single Phospholipid Bilayers. *Phys. Rev. E: Stat. Phys., Plasmas, Fluids, Relat. Interdiscip. Top.* **2000**, *61* (5), 5634−5639.
(81) Dallin, B. C.; Van Lehn, R. C. Spatially Heterogeneous Water Properties at Disordered Surfaces Decrease the Hydrophobicity of Nonpolar Self-Assembled Monolayers. *J. Phys. Chem. Lett.* **2019**, *10*, 3991−3997.
(82) Dallin, B.; Yeon, H.; Ostwalt, A. R.; Abbott, N. L.; Van Lehn, R. C. Molecular Order Affects Interfacial Water Structure and Temperature-Dependent Hydrophobic Interactions between Nonpolar Self-Assembled Monolayers. *Langmuir* **2019**, *35*, 2078.
(83) Baryiames, C. P.; Teel, M.; Baiz, C. R. Interfacial H-Bond Dynamics in Reverse Micelles: The Role of Surfactant Heterogeneity. *Langmuir* **2019**, *35*, 11463.

https://dx.doi.org/10.1021/acs.jpcb.0c00490
J. Phys. Chem. B 2020, 124, 3043−3053